IEEE Access
Multidisciplinary | Rapid Review | Open Access Journal

Received 2 August 2022, accepted 19 August 2022, date of publication 25 August 2022, date of current version 1 September 2022.

Digital Object Identifier 10.1109/ACCESS.2022.3201536

APPLIED RESEARCH

Frequency Excursion Likelihood Constrained Resource Scheduling for Large-Scale Renewable Energy Integration

AKILA HERATH[1], (Student Member, IEEE), M. A. MOHAMMED MANAZ[2], (Member, IEEE), KITHSIRI M. LIYANAGE[1], (Senior Member, IEEE), TAISUKE MASUTA[3], (Member, IEEE), CHAN-NAN LU[2], (Fellow, IEEE), AND KOJI NISHIO[3]

[1]Department of Electrical and Electronic Engineering, University of Peradeniya, Peradeniya 20400, Sri Lanka
[2]Department of Electrical Engineering, National Sun Yat-sen University, Kaohsiung 804, Taiwan
[3]Department of Electrical and Electronic Engineering, Meijo University, Nagoya 468-8502, Japan

Corresponding author: M. A. Mohammed Manaz (mohdmanaz@gmail.com)

This work was supported in part by the Taiwan Ministry of Science and Technology under Grant MOST 108-2221-E-110-036-MY3 and Grant MOST 110-2222-E-110-002-MY3, and in part by the Meijo Asian Research Center.

ABSTRACT Net-load variability and uncertainty in high renewable penetration networks have imposed new challenges to the system operators; adequate ramping, restart, and wider frequency and voltage operation capabilities provided by responsive resources are required to preserve acceptable service quality. Flexibility indicators and resource requirement constraints are proposed for unit commitment studies to address fast net-load variations. However, there is a gap in demonstrating the application of proposed flexibility indicators to determine the required minimum cost flexibility reserves to maintain desired operational performance. To address this issue for system operation planning purposes, a two-stage corrective flexibility constrained unit commitment (FCUC) formulation supported by a data-driven scheme for uncertainty quantification of flexibility shortage driven under and over frequency events is proposed. The first stage unit commitment (UC) is solved with relaxed flexibility constraints to determine the nominal resource schedules. A statistical test is used to determine if the second stage UC is needed. The second stage UC is solved with tighter flexibility constraints. A procedure to quantify the additional flexibility resources needed in the second stage UC to achieve adequate frequency regulation performance with lower operational costs is presented. Test results under various operation scenarios and comparisons with previous flexibility deployment methods illustrate the effectiveness of the proposed method. Test results indicate that in certain situations, flexible resources should remain online and be prioritized against less flexible (although cheaper) resources. The costs incurred by the additional system flexibility required to maintain good frequency control performance can be evaluated.

INDEX TERMS Flexibility, flexibility constraints, renewable energy, under/over frequency probability, unit commitment.

NOMENCLATURE

A_1, A_2	Numerators resulting from the partial fraction expansion of the transfer function $\Delta f(s)$.
d	The next day for which the operation is planned.
d^h	$d^h \in \Omega$ represents a past day belonging to set Ω.
D	Damping constant of the system.
DT_i	Minimum downtime of unit i.
$f_{\pm}(i,t,d)$	Upward/downward (+/−) flexibility of unit i at hour t of day d.
$\check{f}_{\pm}(i,t,d)$	Auxiliary variables representing the upward and downward (+/−) flexibility required from each unit i at hour t during next day operations.

The associate editor coordinating the review of this manuscript and approving it for publication was Zhouyang Ren.

F_r	Fraction of spinning reserve capacity deliverable readily.
$F_{\pm}(t,d)$	Upward/downward (+/−) flexibility of the system at hour t of day d.
$\hat{F}^{ad}_{\pm}(t,d)$	Upward/downward (+/−) normalized additional flexibility of the system at hour t of day d.
$\hat{F}^{ad}_{\pm,req}(t,d)$	Upward/downward (+/−) normalized additional flexibility needed to achieve an acceptable reduction in under/over frequency probability at hour t during next-day operations.
$F^{ad}_{\pm}(t,d)$	Upward/downward (+/−) additional flexibility of the system at hour t of day d.
$F^{ad}_{\pm,req}(t,d)$	Upward/downward (+/−) additional flexibility required to achieve a desired operation at hour t of next day
H	Total inertia of the system.
i	An index representing each generator.
k_m	Effective gain constant of the aggregated spinning reserve generators
$\text{Load}(t,d)$	Forecasted Load for hour t of day d.
n	An index representing a possible realization of net-load profile.
$\text{NL}(t,d)$	Forecasted net-load for hour t of day d.
$\text{NLR}_{\pm}(t,d)$	Forecasted 1-hour upward/downward (+/−) net-load ramp for hour t of day d.
$\Delta\text{NLR}_{\pm}(t,d)$	1-hour upward/downward (+/−) net-load ramp deviation from the forecast for hour t of day d.
$\text{OL}(i,t,d)$	Online status of unit i at hour t of day d. (1 if it is online, 0 otherwise).
p_1, p_2	Poles of the transfer function $\Delta f(s)$.
$P(i,t,d)$	Scheduled power of unit i for hour t of day d.
$P_{min}(i)$	Minimum output power limit of unit i.
$P_{max}(i)$	Maximum output power limit of unit i.
$P_{LFC}(i)$	Frequency regulation reserve capacity committed from unit i.
R	Equivalent system droop
R_{load}	Frequency regulation reserve as a percentage of the load.
$\text{RES}(t,d)$	Forecasted RES generation for hour t of day d.
$\text{RR}(i,t,d)$	Ramp rate of unit i during hour t of day d.
$\text{RR}_{\text{min}}(i)$	Minimum ramp rate capacity of unit i.
$\text{RR}_{\text{max}}(i)$	Maximum ramp rate capacity of unit i.
t	Time in hours.
Δt	Duration of unit commitment interval.
T_r	Reheat time constant.
$u(\tau)$	Unit step function.
UT_i	Minimum uptime of unit i.
τ	Time elapsed from the power mismatch event.
Ω	Set of historical days having similar characteristics to the next day operations.
${}^n\#(\cdot)$	Represents a variable $\#(\cdot)$ associated with n^{th} randomly generated net-load realization.
$\#(\cdot)'$	Represents the actual value of the forecasted value given by variable $\#(\cdot)$

I. INTRODUCTION

As the electricity generation moves towards cleaner renewable energy sources (RES), their inherent variable and random nature pose new challenges to the power system operators. In the past, the power system operation involved committing generation capacity and ramping capability to meet relatively smooth and predictable daily load demands. Whereas today, due to intra-day variations of RES and mismatch between the peak load and peak RES output hours, it would require the system operators to repeatedly ramp down and ramp up power outputs from energy resources to match the net-load variations. The increased variability (due to the diurnal nature of RES and load) and uncertainty (caused by load and RES forecast errors) of the net-load, and the replacement of traditional units by inverter-based renewables, would require an improved scheduling algorithm to optimally dispatch flexible resources to balance the net-load (the load not served by the renewable energy sources) variations.

The ability of a power system to deploy its resources to respond timely to net-load changes is called the power system's flexibility [1], [2], [3], [4], [5], [6]. It is reported that when adding 14.5 GW of solar generation to the Electric Reliability Council of Texas (ERCOT) power system, the flexibility requirement could increase for the 1-hour ramp by 135% and for the 3-hour ramp by 30% [1]. It is predicted that for 100% renewable electricity supply scenarios in 2030 and 2050, a generation mix with a nominal capacity of more than twice the maximum demand is required [2] to ensure reliable operations. Failing to meet the system flexibility requirements would lead to frequency deviations and excessive use of frequency regulation resources [7]. Contingency reserve capacity determined in security-constrained unit commitment (SCUC) algorithms [8], [9], [10] must be supplemented with flexibility reserves to ensure net-load following capability amid increased variability and uncertainty.

Scheduling excessive flexibility reserves to support the largest net-load ramps would increase operating costs. To achieve efficient operations, system operators need a tool to find a tradeoff between "low risk- high operation cost options" and "high risk- low operation cost options" and quantify the operation cost impact of flexibility reserve shortage to make a sound decision.

Several flexibility metrics, such as periods of flexibility deficit (PFD), insufficient ramp resource expectation (IRRE),

etc., are proposed in the literature to assist power system planning studies [2], [11], [12], [13], [14], [15], [16], [17]. These metrics give a statistical estimate of the flexibility shortage in terms of rate of occurrence and expectation. Other flexibility metrics, such as normalized flexibility index, measure the generator unit-wise flexibility and are aggregated to get a system-wise figure [18], [19], [20].

A flexibility shortage can result in a power imbalance and affect the system frequency quality [21]. The swing equation describes the relationship between the power mismatch (ΔP) on the system frequency (f),

$$\frac{2H}{f}\frac{df}{dt} = \Delta \mathrm{P} + \Delta \mathrm{P}_{\mathrm{Gov}} + \Delta \mathrm{P}_{\mathrm{D}} \tag{1}$$

$$\Delta \mathrm{P}_{\mathrm{Gov}} = \mathrm{Gov} \times \frac{\Delta \mathrm{f}}{f} \tag{2}$$

$$\Delta \mathrm{P}_{\mathrm{D}} = D \times \frac{\Delta \mathrm{f}}{f} \tag{3}$$

where Δf is the frequency deviation and H is the effective inertia constant of the system. Gov and D represent the coefficients of post-event responses of the generators' primary controls and frequency-dependent load, respectively. The H and Gov depend on the inertia of online generators and their specified control schemes.

Decline of system inertia is causing serious operational concerns with integration of renewables into the main grid. Utilities are making greater efforts to reduce extended frequency excursions. Fig. 1 shows the distributions of frequency observed in Taiwan power system in November of 2003 and March 2022. The statistical grid frequency oscillations around the nominal value may not always follow the expected Gaussian distribution. Several factors contribute to frequency deviations. Measurements showed larger fluctuations every 15 minutes which is the time frame of power dispatch in electricity markets. These can be reduced by adopting shorter dispatch intervals. Abrupt weather condition, out-of-service, and disconnection of local power grid with high renewable energy and the mains would cause high frequency fluctuation risks on the operation day. Sufficient frequency response reserve allocation is necessary to contain the frequency deviation during such contingencies. Net-load forecast error could lead to extended frequency excursions if the system lacks flexibility.

Economic dispatch formulations that maximize flexibility reserve to respond to the uncertainty of forecasted RES generation variations are presented in [22], [23], [24], and [26]. However, these studies do not provide a direct control mechanism to optimize the desired operational performance.

Previous approaches set minimum required flexibility reserve levels (or flexibility margins) to cover an accepted portion of the historical net-load forecast error distribution or to support a set of forecast error scenarios generated using historical net-load forecast error distribution.

Some UC/ED formulations set the minimum flexibility reserve margins (Flex_up, Flex_down in Fig. 2) higher than predefined forecast error confidence to reduce the variance

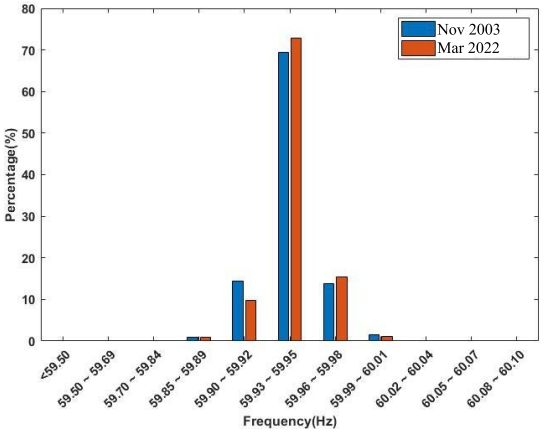

FIGURE 1. Distribution of frequency deviations observed in Taiwan power system in November of 2003 and March of 2022.

of the power mismatch distribution. This approach would lead to increased operational costs due to conservative estimates of the largest acceptable power mismatch. Relaxing the flexibility constraints in the UC formulation to allow some power mismatch events, as long as the frequency deviation is contained within the acceptable limits ($\Delta \mathrm{f}_{\mathrm{min}}$, $\Delta \mathrm{f}_{\mathrm{max}}$) could lower ancillary service costs in renewables integrations.

A flexibility metric suited for operational studies to reflect the effects of flexibility reserve shortage on frequency deviations is yet to be specified. It should provide an avenue for the operators to improve their unit commitment/dispatch decisions to achieve acceptable performance and costs. In this paper, the relationship between under/over frequency probability and normalized additional flexibility via F^2P-maps is determined and a statistical analyses based two-stage UC method is proposed to determine adequate minimum cost flexibility reserves needed to improve the frequency control performance when excessive frequency violation is foreseen. The first UC stage is solved with relaxed flexibility constraints to determine the next-day nominal schedule. A statistical analysis based on next-day unit schedule and historical net-load variations is used to predict if the second stage corrective UC is required. If needed, the statistical analyses results are extrapolated to determine the additional flexibility required, and the corrective UC stage is solved with tighter flexibility constraints to improve flexibility provision. The contributions of this paper are:

i. Devising a corrective flexibility constrained unit commitment (FCUC) formulation to improve the next-day generation schedule when predicted frequency violation probability exceeds the acceptable limit.
ii. Introducing a stochastic approach to establish the connection between flexibility reserve shortage and under/over frequency probability.
iii. Proposing a method to quantify additional flexibility resources needed to achieve an acceptable frequency regulation performance with lower costs.

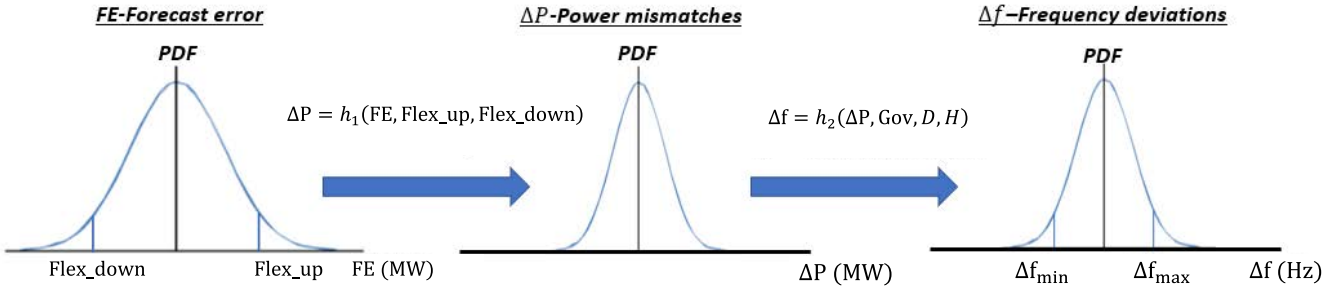

FIGURE 2. Typical Probability distributions of forecast error, power mismatch and frequency deviation obtained by an hour's historical data of a power system.

The rest of this paper is organized as follows. Section II gives a concise account of flexibility evaluation. Section III presents the proposed FCUC formulation and its constituents. Numerical results are given in Section IV, and Section V has the concluding remarks.

II. FLEXIBILITY RESOURCE SCHEDULING

Operational flexibility represents the system's ability to deploy its resources to balance the changes in the net-load. It depends on several factors, such as the ramping, quick-start, and cycling capability of the available resources, control margin available to adjust the power outputs, operational practices (e.g., look ahead unit commitment and economic dispatch can be more effective at responding to net-load variations compared to their conventional variants), and emission and cost considerations [23]. In this work, flexibility limitations due to emission and cost considerations, and the effects of operational practices on flexibility are not explicitly considered.

We utilize the system flexibility deployments and the frequency responses obtained for past operation scenarios to model the nominal relationship between flexibility and frequency deviations. If likelihood of large frequency deviations is low, the operators could reduce the flexibility reserve deployment to save operation costs.

The magnitude of power mismatch, available frequency response reserves, and system inertia in different periods of a day and different seasons would determine severity of the frequency deviations. The operation flexibility contributed by online energy resources is evaluated first by quantifying the range of power adjustment (up and down) available from each energy resource i (i.e., $C = [f_-(i,t,d), f_+(i,t,d)]$) over a given time horizon Δt(in hours), and then by aggregating them (also referred to as ''available flexibility'' or ''flexibility envelop'') [2], [25], [27]. The up and down adjustment ranges of a generator can be found using (4) and (5).

$$f_+(i,t,d) = \mathrm{OL}(i,t,d) \times \min\{(\mathrm{RR}_{\max}(i) \times \Delta\mathrm{t}), ((P_{max}(i) - P_{LFC}(i)) - P(i,t,d))\} \quad (4)$$

$$f_-(i,t,d) = \mathrm{OL}(i,t,d) \times \min\{(\mathrm{RR}_{\min}(i) \times \Delta\mathrm{t}), (P(i,t,d) - (P_{min}(i) + P_{LFC}(i)))\} \quad (5)$$

For a system with q number of generators, its total Δt-hour flexibility at time t of day d is defined by,

$$F_+(t,d) = \sum_{i=1}^{i=q} f_+(i,t,d) \quad (6)$$

$$F_-(t,d) = \sum_{i=1}^{i=q} f_-(i,t,d) \quad (7)$$

System operators perform the next-day unit commitment based on the forecasted net-load profile. If the forecast is accurate, the operators could precisely determine the flexibility required to cope with the forecasted net-load variations. However, due to possible rough weather conditions in a high renewable energy power system, the net-load forecast error could be significant. This uncertainty may require the operators to schedule additional flexibility reserves to manage possible net-load deviations away from the forecasted values.

The forecasted upward and downward Δt hour net-load ramps at hour t are,

$$\mathrm{NLR}_+(t,d) = \max\{\mathrm{NL}(t+\Delta\mathrm{t},d) - \mathrm{NL}(t,d), 0\} \quad (8)$$

$$\mathrm{NLR}_-(t,d) = \max\{\mathrm{NL}(t,d) - \mathrm{NL}(t+\Delta\mathrm{t},d), 0\} \quad (9)$$

where, $\mathrm{NL}(t,d) = \mathrm{Load}(t,d) - \mathrm{RES}(t,d)$ is the forecasted net-load for hour t of day d.

Let $\mathrm{NL}'(t,d) = \mathrm{Load}'(t,d) - \mathrm{RES}'(t,d)$ represent the actual net-load during operation day d at hour t, then the actual effective net-load ramps different from the forecasted net-load ramps can be expressed as:

$$\mathrm{NLR}'_+(t,d) = \max\{\mathrm{NL}'(t+\Delta\mathrm{t},d) - \mathrm{NL}(t,d), 0\} \quad (10)$$

$$\mathrm{NLR}'_-(t,d) = \max\{\mathrm{NL}(t,d) - \mathrm{NL}'(t+\Delta\mathrm{t},d), 0\} \quad (11)$$

When the uncertain upward or downward net-load ramp deviations ($\Delta\mathrm{NLR}_\pm(t,d)$) defined as

$$\Delta\mathrm{NLR}_+(t,d) = \mathrm{NLR}'_+(t,d) - \mathrm{NLR}_+(t,d) \quad (12)$$

$$\Delta\mathrm{NLR}_-(t,d) = \mathrm{NLR}'_-(t,d) - \mathrm{NLR}_-(t,d) \quad (13)$$

exceed a certain threshold, the frequency control performance may degrade, and additional flexibility is required. Past observations of under and over frequency events associated

with flexibility shortage can be analyzed to assist informed decision-making on flexibility resource re-scheduling if desirable.

III. OPERATIONAL PERFORMANCE BASED FLEXIBILITY RESERVE EVALUATION AND CORRECTIVE SCHEDULING

In this paper, a two-stage unit commitment procedure is proposed to optimize flexibility reserve scheduling. The first UC stage is solved with relaxed flexibility constraints to determine the next-day nominal schedule. A statistical analysis based on the obtained nominal next-day unit commitment schedule and historical net-load variations is used to predict if the second stage corrective UC is required. If needed, the statistical analysis results are extrapolated to determine the additional flexibility required, and the corrective UC stage is solved with tighter flexibility constraints to enhance flexibility provision.

A. FLEXIBILITY CONSTRAINED UNIT COMMITMENT (FCUC)

The proposed formulation incorporates additional linear flexibility constraints (14)-(19) in the original UC formulation (given in Appendix A) [28], [29] to deploy a predetermined amount of flexibility reserve.

$$\sum_{i=1}^{i=q} \breve{f}_{+}(i,t,d) \geq \mathrm{NLR}_{+}(t,d) + F^{ad}_{+,req}(t,d) \tag{14}$$

$$\sum_{i=1}^{i=q} \breve{f}_{-}(i,t,d) \geq \mathrm{NLR}_{-}(t,d) + F^{ad}_{-,req}(t,d) \tag{15}$$

$$\breve{f}_{+}(i,t,d) \leq \mathrm{OL}(i,t,d)\,(\mathrm{RR}_{\max}(i) \times \Delta\mathrm{t}), \quad \forall i \tag{16}$$

$$\breve{f}_{+}(i,t,d) \leq \mathrm{OL}(i,t,d)\,(P_{max}(i) - P_{LFC}(i) - P(i,t,d)), \quad \forall i \tag{17}$$

$$\breve{f}_{-}(i,t,d) \leq \mathrm{OL}(i,t,d)\,(\mathrm{RR}_{\min}(i) \times \Delta\mathrm{t}), \quad \forall i \tag{18}$$

$$\breve{f}_{-}(i,t,d) \leq \mathrm{OL}(i,t,d)\,(P(i,t,d) - P_{min}(i) - P_{LFC}(i)), \quad \forall i \tag{19}$$

where, $\breve{f}_{+}(i,t,d), \breve{f}_{-}(i,t,d) \geq 0$ are auxiliary variables representing the upward and downward flexibility required from each resource i at hour $t \in [1,24]$. The constraints (14), and (15) enforce the system flexibility requirements by limiting sum of $\breve{f}_{\pm}(i,t,d)$ to be larger than the forecasted net-load ramps plus the required additional flexibility ($F^{ad}_{\pm,req}(t,d)$). Constraints (16)-(19) enforce upper bounds on $\breve{f}_{+}(i,t,d)$ and $\breve{f}_{-}(i,t,d)$ based on the individual resource capability.

The flexibility constraints are relaxed in the first UC stage by setting the $F^{ad}_{\pm,req}(t,d) = 0 \forall t \in [1,24]$ in (14) and (15). Statistical analysis described in the next subsection is used to predict the next-day frequency control performance. If the predicted frequency control performance is not acceptable, the FCUC is executed with appropriate values for $F^{ad}_{\pm,req}(t,d)\,\forall t \in [1,24]$. The procedure is described in Section III(C).

B. ESTMATION OF FREQUENCY VIOLATION PROBABILITY

In fig. 3, a Monte-Carlo simulation procedure based on historical operation data showcases the major steps involved in estimating probability of large frequency deviation during an operation day d. To simplify the presentation, we will assume $\Delta\mathrm{t} = 1\ hour$.

Step 1: Solve the FCUC program with relaxed flexibility constraints (i.e., $F^{ad}_{\pm,req}(t,d) = 0 \forall t \in [1,24]$ in (14) and (15)) to determine the units' nominal power output schedule.

Step 2: Calculate the available additional flexibility, $F^{ad}_{\pm}(t,d)$, at each hour $t \in [1,24]$ (20).

$$F^{ad}_{\pm}(t,d) = F_{\pm}(t,d) - \mathrm{NLR}_{\pm}(t,d) \tag{20}$$

To maintain proper operations the available additional flexibility at hour t should be sufficient to meet the unforeseen net-load deviations caused by RES forecast errors. For the subsequent analysis the normalized additional flexibility is computed as in (21),

$$\hat{\mathrm{F}}^{ad}_{\pm}(t,d) = \left(\frac{F^{ad}_{\pm}(t,d)}{\mathrm{RES}(t+1,d)+1}\right) \tag{21}$$

(In the denominator, 1 MW is added to the RES forecast to avoid it becoming zero).

Step 3: Perform Monte-Carlo simulations considering N number of possible realizations of the actual net-load (generated by sampling the forecast error distribution. Refer to Appendix B for information on the forecast error distributions) and determine if there is any time instance with flexibility shortage; if there are flexibility shortages, then compute the resulting maximum system frequency deviations due to that shortage. The maximum frequency deviation is computed using the following simplified frequency response (SFR) model [30].

$$\Delta\mathrm{f}(s) = \frac{1}{2\pi}\left(\frac{{}^{n}\Delta\mathrm{P}_0(s)(1+T_r s)}{(2Hs+D)(1+T_r s)+\frac{k_m}{R}(1+F_r T_r s)}\right) \tag{22}$$

$${}^{n}\Delta\mathrm{f}(t,d,\tau) = {}^{n}\Delta\mathrm{P}_0(t,d)\frac{1}{2\pi}\left(\frac{A_1}{p_1}\left(1-e^{p_1\tau}\right)u(\tau) + \frac{A_2}{p_2}\left(1-e^{p_2\tau}\right)u(\tau)\right) \tag{23}$$

where, ${}^{\mathrm{n}}\Delta\mathrm{P}_0(t,d)$ is the power mismatch (due to flexibility shortage) at the end of hour t in the n^{th} random net-load realization. It is calculated by the following:

$${}^{n}\Delta\mathrm{P}_0(t,d) = \begin{cases} {}^{n}\Delta\mathrm{NLR}_{+}(t,d) - F^{ad}_{+}(t,d); \\ \quad {}^{n}\Delta\mathrm{NLR}_{+}(t,d) > F^{ad}_{+}(t,d) \\ F^{ad}_{-}(t,d) - {}^{n}\Delta\mathrm{NLR}_{-}(t,d); \\ \quad {}^{n}\Delta\mathrm{NLR}_{-}(t,d) > F^{ad}_{-}(t,d) \\ 0; \quad Otherwise \end{cases} \tag{24}$$

The maximum frequency deviation (${}^{n}\Delta\mathrm{f}_{\mathrm{nadir}}(t,d)$) is computed by setting the gradient $\frac{d({}^{n}\Delta\mathrm{f}(t,d,n,\tau))}{d\tau}$ to zero and finding the corresponding frequency value.

The stochastically generated N number of net-load realizations for each hour model uncertainties in the net-load. At each hour, every net-load realization's power mismatch and possible frequency deviation estimated by SFR model are calculated. With this scheme, the nature of short-term stochastic frequency response and the near-term operation behavior of the system could be considered in the day-ahead UC program. Different frequency quality requirement level could be specified in the day-ahead UC program. To be conservative, the largest power imbalance caused by flexibility shortage during an hour could be considered to estimate the largest frequency deviation caused by the shortage. In this formulation we consider the 1-hour net-load ramp and flexibility; the method can be extended to include shorter time horizons too.

Step 4: For each hour t, count the total number of net-load realizations resulting in over-frequency or under-frequency situations (based on predefined acceptable frequency limits). Then the over/under frequency probability (OFP/UFP) for each hour is computed by (25) and (26). The UFP and OFP are graphically illustrated on a PDF plot in Fig. 4.

$$\mathrm{OFP}\,(t,d) = \frac{1}{N}\sum_{n=1}^{N}\left({}^{n}\Delta \mathrm{f}_{\mathrm{nadir}}(t,d) > \Delta \mathrm{f}_{\max}\right) \times 100\% \tag{25}$$

$$\mathrm{UFP}(t,d) = \frac{1}{N}\sum_{n=1}^{N}\left({}^{n}\Delta \mathrm{f}_{\mathrm{nadir}}(t,d) < \Delta \mathrm{f}_{\min}\right) \times 100\% \tag{26}$$

C. DEVELOPMENT OF THE F²P-MAP AND ITS APPLICATION IN THE PROPOSED METHOD

Deficiency in upward/downward flexibility would increase the likelihood of under/over frequency situations. Here 'likelihood' refers to the probability of the system frequency exceeding an acceptable preset limit. Based on past operational practices and recorded data, the flow chart shown in fig. 5 determines the mapping between downward (*upward*) normalized additional **F**lexibility and over (*under*) **F**requency violation **probability** (F^2P-map – read as "F to P map") that indicates the relationship between under/over frequency probability and flexibility. Fig. 6 describes the parameters involved in this process. The major steps to develop the F^2P-maps are described below.

Step 1: Select a suitable set of historical days (Ω) that has similar characteristics to the next day's operations (e.g., if the next day is a regular sunny weekday in July, then we may select the operational data corresponding to the similar days of July in previous years). Recorded historical load and renewable generation data corresponding to the selected days ($d^h \in \Omega$) are linearly scaled to match with the current system peak load demand and RES penetration and used in the subsequent steps.

Step 2: Apply the procedure given in Fig. 3 for each day; determine the nominal day-ahead unit schedules and dispatch for each of the selected days using the FCUC formulation presented previously, with the additional flexibility requirement set to zero ($F^{ad}_{\pm,req}(t) = 0$). Calculate under/over frequency probability and normalized additional flexibilities for each hour.

Step 3: Determine the relationship between the over/under frequency probability and normalized additional flexibility. Two scatter graphs G^t_+ and G^t_- for each hour $t \in [1, 24]$ by grouping the output obtained in step 3 corresponding to hour t of all days in Ω can be obtained. Each scatter graph corresponding to hour t would contain all the following data points:

$$G^t_+ \Longrightarrow \left(\hat{\mathrm{F}}^{ad}_+\left(t,d^h\right), \mathrm{UFP}\left(t,d^h\right)\right) \quad \forall d^h \in \Omega$$

$$G^t_- \Longrightarrow \left(\hat{\mathrm{F}}^{ad}_-\left(t,d^h\right), \mathrm{OFP}\left(t,d^h\right)\right) \quad \forall d^h \in \Omega$$

By applying piecewise nonlinear regression to each scatter graph, the F^2P-maps are found for each hour t (i.e., $g^t_+ : \hat{\mathrm{F}}^{ad}_+(t) \rightarrow \mathrm{UFP}(t)$ and $g^t_- : \hat{\mathrm{F}}^{ad}_-(t) \rightarrow \mathrm{OFP}(t)$). Different F^2P-maps can be drawn to incorporate operation schemes and weather conditions in different seasons using appropriate historical operational data.

Fig. 7 shows an application example of an upward F^2P-map (i.e., g^t_+); the blue line is the piecewise nonlinear regression function obtained in Step 3. The arrows (i) & (ii) show the steps to find the normalized additional flexibility required ($\hat{\mathrm{F}}^{ad}_{+,req}(t,d)$) to reduce under-frequency probability to an acceptable level $\mathrm{UFP}_{max}(t)$ set by the regulator.

After UFP and OFP for each hour are estimated for the next day, if they are larger than acceptable probability value for some $t \in [1, 24]$, then by using F^2P-map, the amount of normalized additional hourly flexibility requirement ($\hat{\mathrm{F}}^{ad}_{+,req}(t,d)$) to reduce the probability to an acceptable level (e.g., 1%) can be obtained. $F^{ad}_{\pm,req}(t,d)$ for each hour is then computed using the inverse of the definition in (21),

$$F^{ad}_{\pm,req}(t,d) = \hat{\mathrm{F}}^{ad}_{\pm,req}(t) \times (\mathrm{RES}\,(t+1,d)+1) \tag{27}$$

D. APPLICATION OF THE PROPOSED UC METHOD IN POWER SYSTEM OPERATIONS

The application of the proposed UC method in power system operation framework has mainly three steps: 1) generate F^2P-maps using past net-load data, 2) use the first-stage UC to identify excessive frequency excursions caused by flexibility shortage, and 3) if needed, revise the resource schedule using the second-stage UC.

The 1st step involves selecting a suitable set of historical operation data and performing the Monte-Carlo simulations as described in Section III(C). This step can be performed before solving next day UC schedule. The 2nd step is solving the FCUC for the forecasted next day net-load with relaxed flexibility constraints. The nominal UC schedules obtained in this stage are analyzed to determine the likelihood of frequency violations during next day operation (using the method described in Section III(B)). Depending on the number of scenarios considered in the Monte-Carlo simulations,

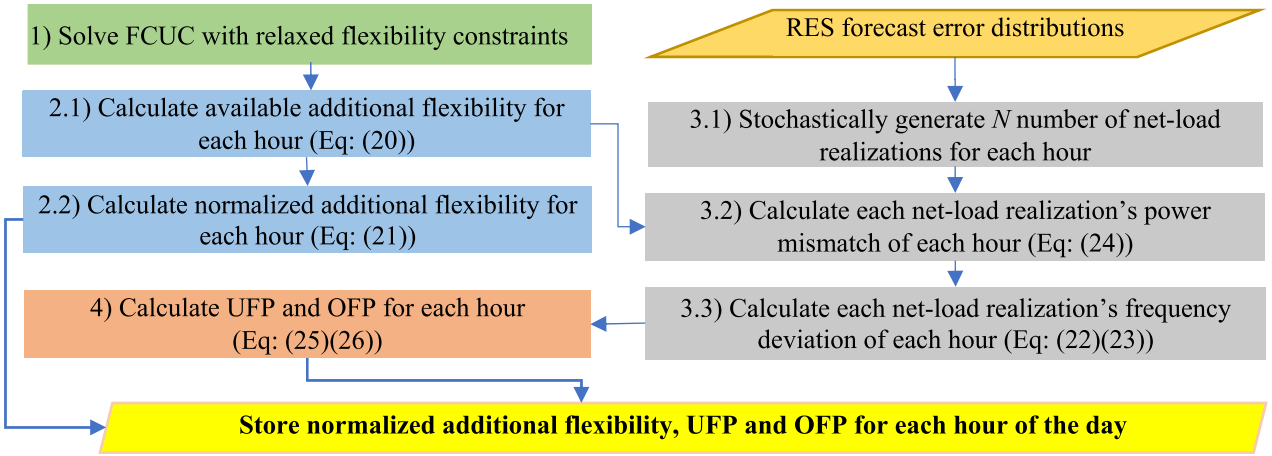

FIGURE 3. Flow diagram of the proposed method to determine under/over frequency probability and normalized additional flexibility of next day.

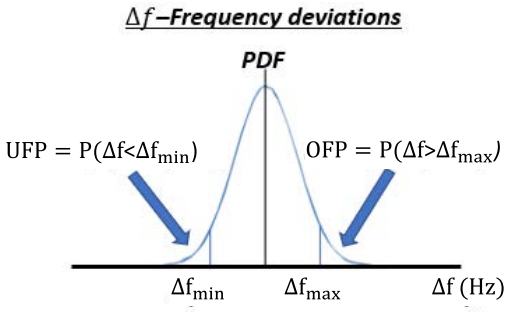

FIGURE 4. Graphical illustration of UFP and OFP.

size of the system, and renewable energy penetration level, the execution time needed for developing the F^{2}P-maps may vary. A system with high-RES content and low net-load would require a higher execution time compared to the same system with low- RES content and high net-load. In our tests, it took about 4 hours and 10 hours to compute the F^{2}P-maps in case 1 and case 2, respectively, using a computer equipped with Intel®Core^{TM}i5-4200U processor and 4 GB RAM. These computations can be performed independently and stored for later use in Step 3.

If the predicted frequency violation probability is higher than the acceptable level, the 3rd step is executed to reduce frequency violation probability by enforcing the flexibility constraints in FCUC formulation presented in Section III(A). The minimum flexibility needed to achieve the desired frequency response performance is identified using the F^{2}P-maps (as described Section III(C)).

IV. SIMULATION RESULTS

The power system model of the Kanto area of Japan is used in this study [28]. The maximum demand in this test system is approximately 60 GW. The system consists of 168 dispatchable thermal generators and un-dispatchable nuclear, hydropower sources, and Solar PV. The parameters used in the tests are given below [28], [31].

The test system operates at a nominal frequency of 50 Hz. Acceptable frequency range in these simulations is ±0.3Hz. The frequency response characteristic parameters in (22) are chosen as follows: time constant $T_r = 8$s, system complement fraction $F_r = 0.3$, load damping $D = 1$, system regulation $R = 0.05$, effective gain constant $k_m = 0.95$. Unit commitment interval $\Delta t = 1$ *hour*, unit commitment duration $T = 24$ *hours*. Parameters of the energy resources are given in Table 1.

Operation data from May of 2016 and 2017 (representing different load and renewable energy profiles and variations) are considered in the base case [32]. The net-load forecast errors at each hour are modeled as normal distributions; their mean and standard deviations are given in Table 2 and (Refer to Appendix B for more details). Proper Ω and N are determined based on historical net-load ramp statistics. The historical operation data recorded during May of previous two years ($|\Omega| = 62$) along with 10000 random net-load deviation profiles ($N = 10000$) are used to develop the F^{2}P-maps. Two different renewable penetration cases are analyzed: **Case 1**: 10 GW (original system) and **Case 2**: 20 GW (the test system is modified by replacing nuclear and hydropower sources with oil-based thermal generators, representing a future scenario).

A. COMPARISON OF TWO_STAGE UC AND CONVENTIONAL UC METHODS

The power system operation on a day in May of 2018 is considered for this demonstration. Fig. 8 shows the next-day RES forecast for the system with 10 GW RES. The load forecast error is neglected in these tests. Fig. 9 shows the proportion of the forecasted next-day net-load that should be balanced by dispatchable resources (in green). The next-day nominal unit schedule is computed based on the forecasted net-load (by solving the first stage of UC with relaxed flexibility constraints). The F^{2}P-maps are obtained for each hour using operation data of the same months in the past two years. The F^{2}P-maps shown in fig. 10(a) indicates that

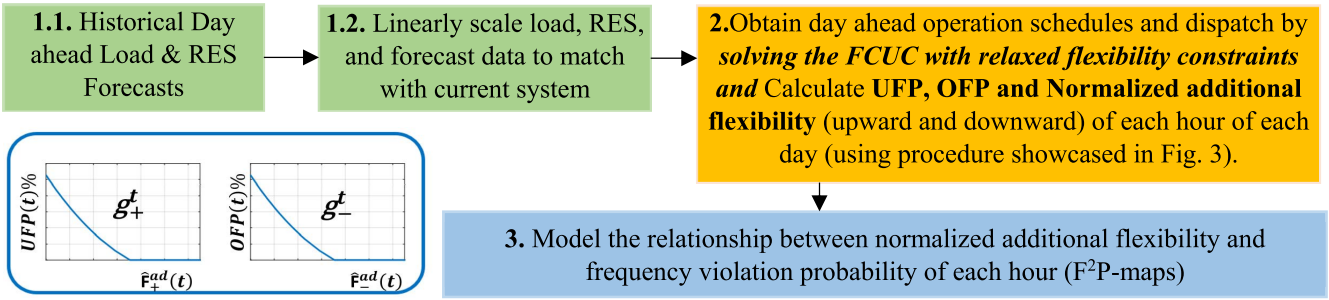

FIGURE 5. Flow diagram to determine the relationship between normalized additional flexibility and frequency violation probability of each hour (F^2P-maps).

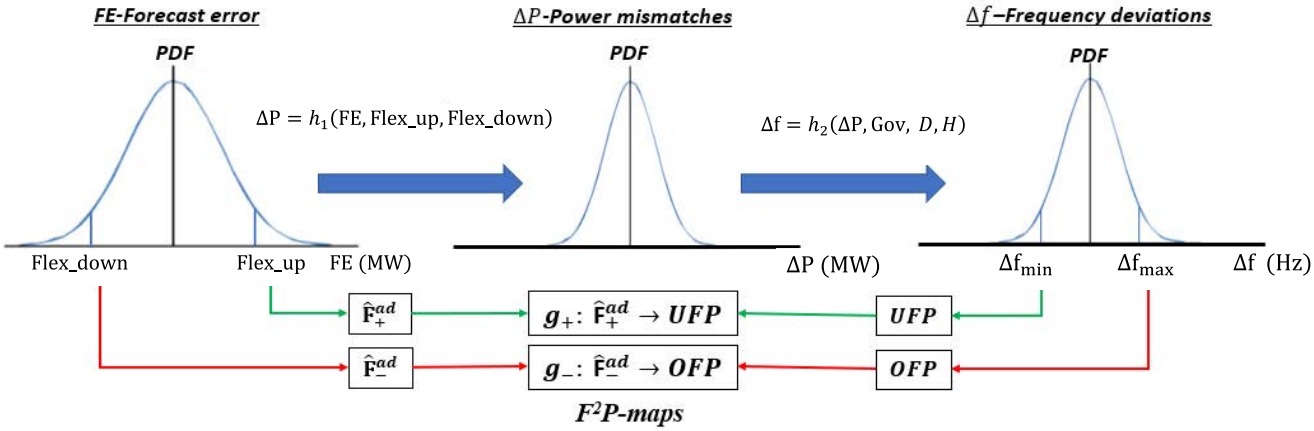

FIGURE 6. Graphical explanation of the parameters involved in F^2P-maps.

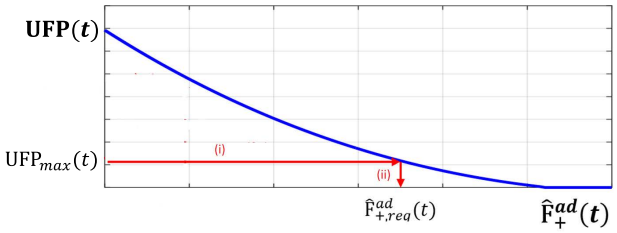

FIGURE 7. Application of F^2P-map to determine the additional flexibility requirement.

between 9.00 am and 1.00 pm, without additional flexibility provision the under-frequency probability could be 17% to 21%. Fig. 10(b) shows that the under frequency probability would further increase in Case 2 due to heightened net-load uncertainty and reduced number of committed thermal units and system flexibility. Over frequency probability of this system is zero for both the test cases and it suggests that the system operates with enough downward flexibility.

To reduce the under frequency probability, the FCUC is applied. The next-day UC of dispatchable thermal generators is determined and compared using 4 UC methods: (i) Conventional UC and FCUC constrained for (ii) 5%, (iii) 1%, (iv) 0% frequency limits violation probability.

The normalized upward additional flexibility during each hour of the day in case 1 dispatched by each of the above four methods are shown in fig. 11. When using the conventional UC method, the additional upward flexibility is low during high-RES generation hours due to fewer dispatchable generators committed. If flexibility reserves are not sufficient the system may be unable to balance the net-load variations. Fig. 12 shows that the predicted next-day under frequency

TABLE 1. Parameters of the energy resources.

	Rated Output (MW)	Lower limit (MW)	Coefficients of Fuel cost function			Startup cost (1000 JPY)	Min. uptime (h)	Min. down-time (h)	Ramp capacity (MW/h)	Inertia (s)	No. of generators
			A	B	C						
			(1000 JPY/h)	(JPY/MWh)	(JPY/MW²h)						
Coal	1000	300	550	400	0.7	2380	8	8	600	3	12
	700	105	182	1300	0.16	1670	6	6	420	3	4
CC	250	63	120	1400	1.66	378	1	1	750	5	74
	100	30	104	900	0.73	151	1	1	300	5	21
LNG	700	140	117	2400	0.4	1060	3	3	1260	4	19
	200	80	66	2200	2.5	302	3	3	350	4	13
Oil	700	175	260	5000	0.38	1060	2	2	1260	2	4
	500	100	200	5000	0.05	756	2	2	900	2	6
	250	50	316	4600	1.05	378	2	2	450	2	15
Hydro	1200	-	-	4000	-	-	-	-	-	4	-
Nuclear	6000	-	-	8000	-	-	-	-	-	8	-
PV	-	-	-	10000	-	-	-	-	-	-	-

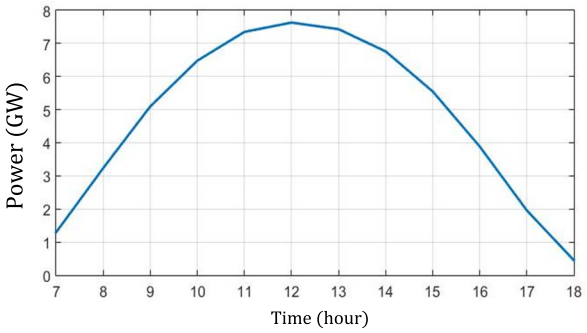

FIGURE 8. Forecasted Renewable generation of 10GW RES system.

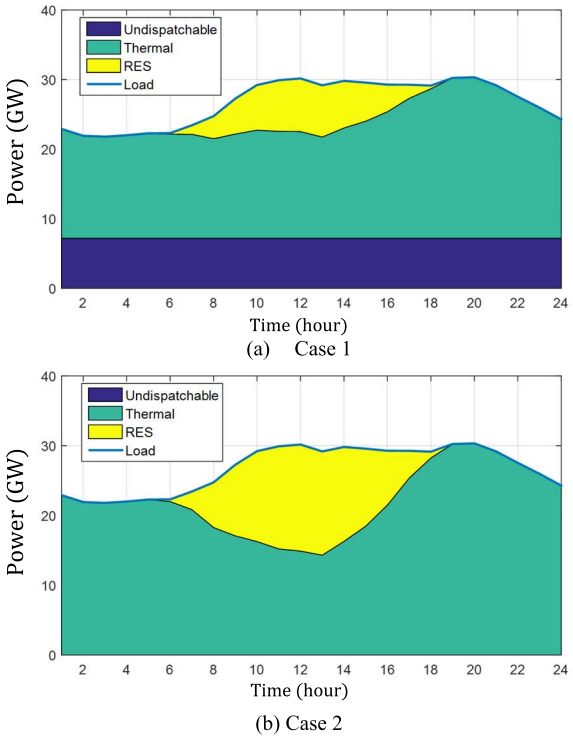

FIGURE 9. Day-ahead forecasts of load and the dispatch proportions of the highest RES generation day in May of the current year.

TABLE 2. Means and standard deviations of normalized RES forecast errors at each hour in may.

Hour	7	8	9	10	11	12	13	14	15	16	17	18
$\sigma(t)$	0.28	0.32	0.30	0.26	0.25	0.40	0.33	0.30	0.28	0.26	0.31	0.29
$\mu(t)$	-0.01	0.05	0.03	0.03	0.02	0.07	0.06	0.08	0.06	0.01	0.00	0.02

probability can reach ∼9% during hour 11 and 13 (due to increased likelihood of power imbalance). The situation is alleviated when using the corrective FCUC; it commits more flexibility reserves compared to conventional UC in hours with high RES forecast uncertainty, which helps to maintain power balance and reduce the predicted next-day under frequency probability. The largest under frequency probability is reduced to 5.3%, 1.3%, and 0%, respectively in each FCUC.

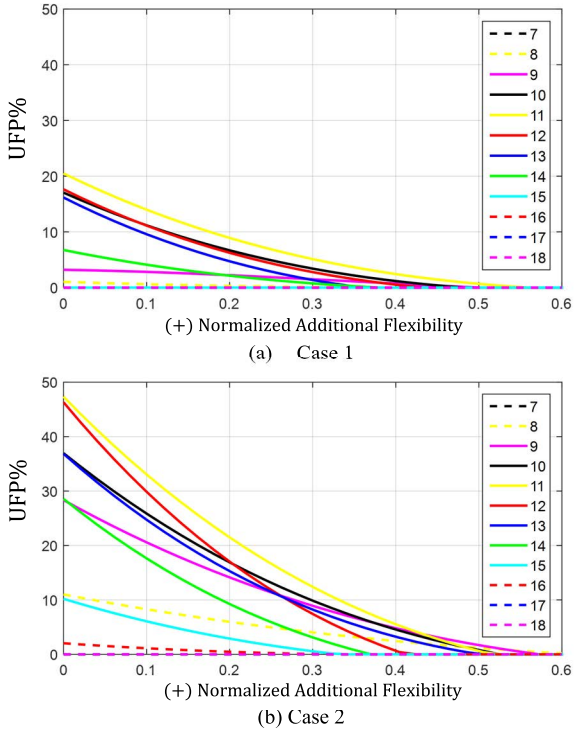

FIGURE 10. F^2P-maps obtained for each hour between 6.00 am and 6.00 pm (given in t: hour number) considering the historical data during the month of May in the previous two years (2016 and 2017).

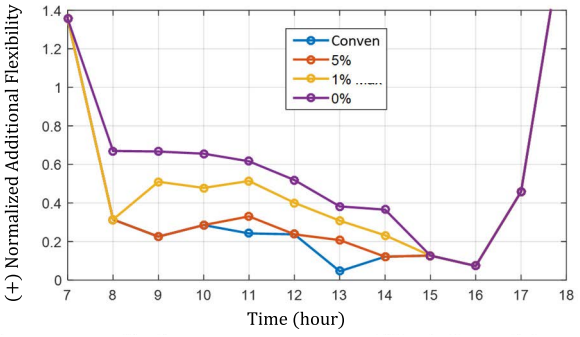

FIGURE 11. Normalized upward additional flexibility during each hour of the day of (case 1).

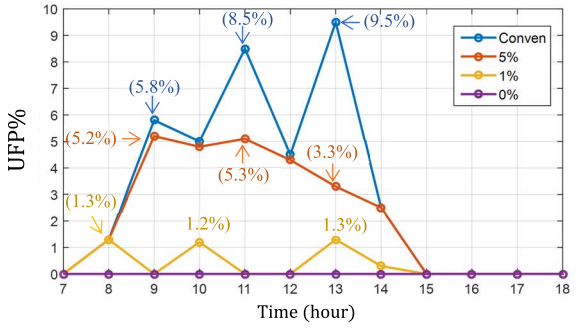

FIGURE 12. Predicted under frequency probability during each hour of the day in (case 1).

To demonstrate the effectiveness of FCUC with maximum frequency violation probability constraints, its application for

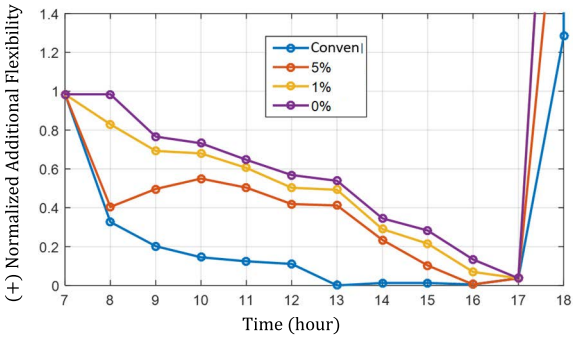

FIGURE 13. Normalized upward additional flexibility during each hour of the day (case 2).

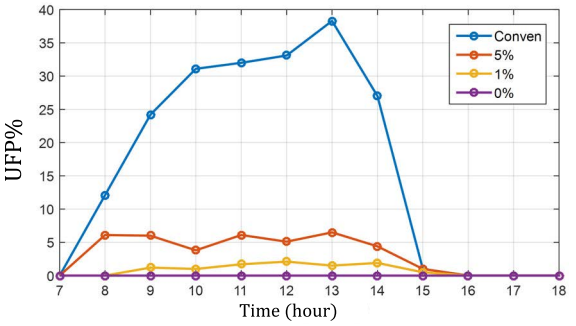

FIGURE 14. Predicted under frequency probability during each hour of the day (case 2).

the same day's operations with case 2 (which has twice the RES capacity) is discussed below. In this case, when using conventional UC, the total number of committed dispatchable generators reduces even further compared to case 1. Normalized additional upward flexibility and the under-frequency probability during the day are shown in fig. 13 and fig. 14, respectively. Compared to case 1, the maximum predicted UFP with conventional UC increases to ∼38%. The UFP is reduced by executing the corrective FCUC.

It should be noted that the proposed F^2P-maps are derived from historical average relationship between additional flexibility and frequency violation probability. The predicted UFP for a future operational day is expected to follow this average trend; nevertheless, some deviations can be expected. Fig. 15 and Fig. 16 show the predicted frequency violation probability for each operational day in May of 2018 when using each UC method in case 1 and case 2 respectively. When using the conventional UC, the highest predicted UFP of ∼18% and 43% is observed during hour 13 in case 1 and case 2. And it is brought under 6% using FCUC with 5% UFP limit. Overall mean and standard deviation of predicted UFP in May of 2018 in case 1 and case 2 are summarized in Table 3 and Table 4, respectively. They show that the algorithm brings the average UFP below the required limits in both cases.

During operations the frequency is expected to remain within the acceptable limits (i.e., ±0.3Hz) with increasing likelihood as we decrease the allowable UFP and OFP. On rare occasions, the frequency may exceed the limits.

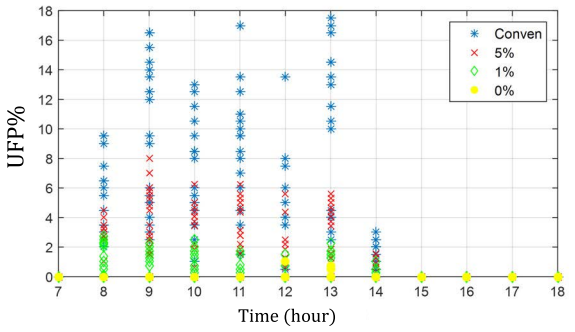

FIGURE 15. Under frequency probability during each hour of all operation day in May of 2018 (case 1).

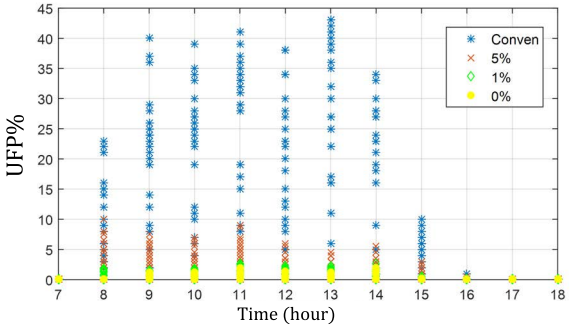

FIGURE 16. Under frequency probability during each hour of all operation day in May of 2018 (case 2).

TABLE 3. Summary of the predicted UFP for all 31 operation days in May of 2018 (case 1).

Time (Hour)		8	9	10	11	12	13	14
Con .UC	Mean (%)	3.32	5.91	4.35	5.16	3.21	6.73	0.94
	St.dev (%)	2.35	5.95	4.15	5.08	1.66	5.65	0.56
FCUC 5%	Mean (%)	1.15	2.66	1.89	1.97	0.70	1.70	0.26
	St.dev (%)	1.54	2.70	2.07	2.10	1.36	2.07	0.50
	No. days above 5%	0	9	2	4	1	3	0
FCUC 1%	Mean (%)	0.66	0.39	0.54	0.20	0.18	0.54	0.08
	St.dev (%)	1.00	0.67	0.81	0.48	0.43	0.76	0.21
	No. days above 1%	9	6	8	3	3	10	1
FCUC 0%	Mean (%)	0.00	0.00	0.00	0.00	0.03	0.10	0.00
	St.dev (%)	0.00	0.00	0.00	0.00	0.18	0.23	0.00
	No. days above 0%	0	0	0	0	1	5	0

B. COMPARISON OF CORRECTIVE FCUC WITH FLEXIBILITY MARGIN CONSTRAINED UC

Operation schedules for case 1 and case 2 for the 31 operations days in May of 2018 are obtained with flexibility margin based UC procedure used in previous studies. Here the probability of power mismatch event (instead of frequency violation) is considered as the limiting parameter. The UC is executed with maximum of 5% and 1% power mismatch probabilities. The required additional flexibility to limit the probability of power mismatches to the desired values at each hour is determined using the net-load forecast error distributions. For an example, to limit maximum upward power mismatch probability to 5%, the required additional upward flexibility ($F^{ad}_{+,req}$) is equal to the positive net-load

TABLE 4. Summary of the predicted UFP for all 31 operation days in May of 2018 (case 2).

Time (Hour)		8	9	10	11	12	13	14
Con .UC	Mean (%)	7.77	17.45	17.45	21.29	16.13	22.29	12.71
	St.dev (%)	7.48	11.91	12.53	14.20	13.01	16.17	12.47
FCUC 5%	Mean (%)	3.13	3.23	2.42	3.13	2.21	1.73	1.63
	St.dev (%)	2.90	2.30	2.08	2.61	1.80	1.52	1.77
	No. days above 5%	7	7	4	6	2	0	2
FCUC 1%	Mean (%)	0.41	0.43	0.50	0.65	0.69	0.56	0.48
	St.dev (%)	0.61	0.61	0.60	0.90	0.75	0.73	0.73
	No. days above 1%	7	8	7	9	10	11	8
FCUC 0%	Mean (%)	0.00	0.19	0.20	0.32	0.18	0.17	0.25
	St.dev (%)	0.00	0.37	0.40	0.59	0.40	0.36	0.59
	No. days above 0%	0	7	7	8	6	6	6

TABLE 5. Comparison of FCUC and other UC results for all 31 operation days in May of 2018.

	UC method	Average no. of Thermal generators committed per hour	Average UFP% per hour	Avg. daily operational cost (JPY million)
Case-1	Conventional	54.79	1.23	1019.50
	FCUC -5% (Freq)	55.00	0.43	1019.63
	FCUC -1% (Freq)	55.61	0.11	1019.69
	FCUC -0% (Freq)	56.39	0.00	1019.81
	FCUC -5% (Power)	58.83	0.00	1020.61
	FCUC -1% (Power)	60.62	0.00	1021.52
Case-2	Conventional	80.36	2.11	1239.81
	FCUC -5% (Freq)	83.36	0.74	1240.59
	FCUC -1% (Freq)	84.73	0.18	1241.12
	FCUC -0% (Freq)	85.17	0.01	1241.52
	FCUC -5% (Power)	88.65	0.00	1242.82
	FCUC -1% (Power)	91.22	0.00	1250.18

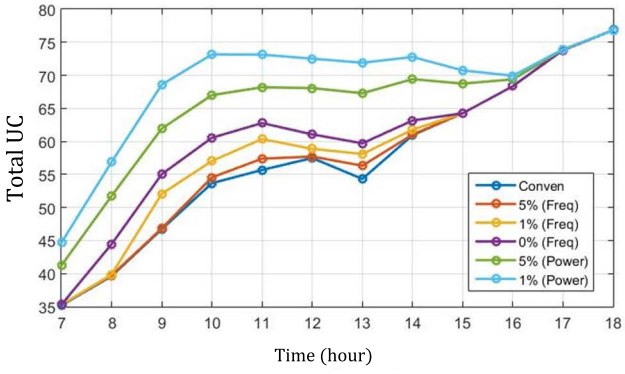

FIGURE 17. Average number of dispatchable units committed in case 1 from 6.00 am to 6.00 pm for all the UC schemes considered.

forecast error margin that covers 95% of the net-load forecast error distribution.

Table 5 shows the average number of thermal generators committed, average UFP, and the average daily operational cost under each unit commitment schedule 1 and case 2. The flexibility margin based UC requires more thermal units and incurs a higher operation cost. It shows good frequency regulation with 0% UFP throughout the day. Nevertheless, the

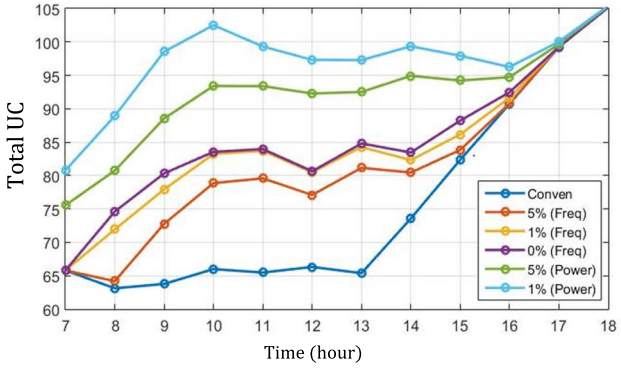

FIGURE 18. Average number of dispatchable units committed in case 2 from 6.00 am to 6.00 pm for all the 6 UC schemes considered.

proposed corrective FCUC with 0% maximum UFP achieves a similar frequency regulation performance at a lower cost. Fig. 17 and Fig. 18 present the average number of dispatchable units committed during each hour between 6.00 am and 6.00 pm in case 1 and case 2 respectively. During certain hours the proposed corrective FCUC method reduces the average number of dispatchable units by more than 10 units while achieving similar frequency regulation performance as the flexibility margin based UC algorithm.

V. CONCLUSION

This paper presents a new flexibility constrained UC formulation; the first UC stage is solved with relaxed flexibility constraints to determine the next-day nominal schedule, and then a corrective UC stage is solved with tighter flexibility constraints if needed. A Monte-Carlo simulation according to next-day unit schedule and historical net-load variations is used to predict if the second stage corrective UC is required. If needed, the F^2P-maps are used to determine the normalized additional flexibility. The corrective UC stage is solved with tighter constraints to improve flexibility provision. The proposed method provides a tool for system operators to optimize the unit commitment schedule while limiting the likelihood of frequency limit violations. F^2P-maps representing the relationship between the available flexibility and under/over frequency probabilities based on past system operation experiences could be applied in a high renewable energy provision environment to perform cost analysis on additional flexibility needed to limit the under and over frequency probability to an acceptable level. The cost saving benefits of the proposed method are compared to the flexibility margin based UC methods. In seasons with higher uncertainty of hourly net-loads, the corrective FCUC scheme could assist system operator to make informed decision on flexibility resource dispatch with lower operation cost.

Flexibility resources requirements of a system must be identified ahead of time and appropriate strategic decisions must be taken at the long-term planning stage. Existing power plants can be retrofitted to increase their ramping capability and quick-start generators could be built to cater the power system flexibility requirements. These issues

have been extensively discussed in the literature and we do not address this issue in this paper. If a system with high renewable energy resources lacks the required flexibility resources, its operations will become increasingly challenging.

This paper proposes a method to optimally schedule the flexibility resources in a power system while achieving an acceptable frequency response performance. If the system does not have enough flexible resources as required by the flexibility constraints, the FCUC program may not find a feasible solution. This can be avoided by converting these constraints into soft constraints by using penalty functions to find the best solution. Appropriate modifications of the proposed method to suite a system lacking flexible resources will be further studied in the future.

APPENDIX A
CONVENTIONAL UC FORMULATION

The formulation presented here is an adaptation of conventional UC found in [29] for the operation procedures of the system discussed in [28].

$$\min_{P(i,t,d)\in\mathbb{R},\mathrm{OL}(i,t,d)\in\{0,1\}} \sum_{t=1}^{t=T}\sum_{i=1}^{i=q}\left\{\begin{array}{l}\mathrm{FC}\left(P\left(i,t,d\right)\right)\mathrm{OL}\left(i,t,d\right)\\ +\mathrm{SC}\left(i\right)\mathrm{OL}\left(i,t,d\right)\left(1-\mathrm{OL}\left(i,t-1,d\right)\right)\end{array}\right\} \tag{A-1}$$

where $A\left(i\right), B\left(i\right), C\left(i\right) \in \mathbb{R}$ are constants, $\mathrm{SC}\left(i\right)$ is the startup cost of unit i. $\mathrm{FC}\left(P\left(i,t,d\right)\right) = A\left(i\right) + B\left(i\right)P\left(i,t,d\right) + C\left(i\right)\left(P\left(i,t,d\right)\right)^2$.

Subject to:

$$\mathrm{NL}\left(t,d\right) = \sum_{i=1}^{i=q} P\left(i,t,d\right) + P_{hydro}\left(t,d\right) + P_{nuclear}\left(t,d\right) \tag{A-2}$$

$$P\left(i,t,d\right) = P\left(i,t-1,d\right) + \mathrm{RR}\left(i,t,d\right)\Delta\mathrm{t} \tag{A-3}$$

$$\left(P_{min}\left(i\right) + P_{LFC}\left(i\right)\right)\mathrm{OL}\left(i,t,d\right) \le P\left(i,t,d\right) \le \left(P_{max}\left(i\right) - P_{LFC}\left(i\right)\right)\mathrm{OL}(i,t,d) \tag{A-4}$$

$$\sum_{i=1}^{i=q} P_{LFC}\left(i\right)\mathrm{OL}\left(i,t,d\right) \ge \mathrm{Load}(t,d)R_{Load} \tag{A-5}$$

$$\mathrm{RR}_{\min}\left(i\right) \le \mathrm{RR}\left(i,t,d\right) \le \mathrm{RR}_{\max}\left(i\right) \tag{A-6}$$

$$\sum_{t=k}^{t=k+\mathrm{UT}_i-1}\mathrm{OL}\left(i,k,d\right) \ge \mathrm{UT}_i\left[\mathrm{OL}\left(i,k,d\right) - \mathrm{OL}\left(i,k-1,d\right)\right], \quad \forall k = 1:\left(T-\mathrm{UT}_i+1\right) \tag{A-7}$$

$$\sum_{t=k}^{t=T}\left\{\mathrm{OL}\left(i,t,d\right) - \left[\mathrm{OL}\left(i,k,d\right) - \mathrm{OL}\left(i,k-1,d\right)\right]\right\} \ge 0, \quad \forall k = \left(T-\mathrm{UT}_i+2\right):T \tag{A-8}$$

$$\sum_{t=k}^{t=k+\mathrm{DT}_i-1}\left(1-\mathrm{OL}(i,k,d)\right) \ge \mathrm{DT}_i\left[\mathrm{OL}\left(i,k-1,d\right) - \mathrm{OL}\left(i,k,d\right)\right], \quad \forall k = 1:\left(T-\mathrm{DT}_i+1\right) \tag{A-9}$$

$$\sum_{t=k}^{t=T}\left\{1-\mathrm{OL}\left(i,t,d\right) - \left[\mathrm{OL}\left(i,k-1,d\right) - \mathrm{OL}\left(i,k,d\right)\right]\right\} \ge 0, \quad \forall k = \left(T-\mathrm{DT}_i+2\right):T \tag{A-10}$$

APPENDIX B
FORECAST ERROR DISTRIBUTION

By using the historical RES forecasts and actual RES generation data, the RES forecast error ($\in_{\mathrm{RES}}(t,d^h)$) for each hour are calculated by applying the following equation.

$$\in_{\mathrm{RES}}\left(t,d^h\right) = \left(\frac{\mathrm{RES}'(t,d^h) - \mathrm{RES}(t,d^h)}{\mathrm{RES}(t,d^h)}\right) \tag{B-1}$$

The forecast error corresponding to each hour is stochastically modeled as normally distributed random variable mean $\mu(t)$ and standard deviation $\sigma\left(t\right)$.

REFERENCES

[1] H. Holttinen, A. Tuohy, M. Milligan, E. Lannoye, V. Silva, S. Müller, and L. Soder, "The flexibility workout: Managing variable resources and assessing the need for power system modification," *IEEE Power Energy Mag.*, vol. 11, no. 6, pp. 53–62, Nov. 2013, doi: 10.1109/MPE.2013.2278000.
[2] E. Lannoye, D. Flynn, and M. OMalley, "Evaluation of power system flexibility," *IEEE Trans. Power Syst.*, vol. 27, no. 2, pp. 922–931, May 2012, doi: 10.1109/TPWRS.2011.2177280.
[3] E. Lannoye, D. Flynn, and M. O'Malley, "The role of power system flexibility in generation planning," in *Proc. IEEE Power Energy Soc. Gen. Meeting*, San Diego, CA, USA, Jul. 2011, pp. 1–6, doi: 10.1109/PES.2011.6039009.
[4] A. Akrami, M. Doostizadeh, and F. Aminifar, "Power system flexibility: An overview of emergence to evolution," *J. Modern Power Syst. Clean Energy*, vol. 7, no. 5, pp. 987–1007, Sep. 2019, doi: 10.1007/s40565-019-0527-4.
[5] B. Mohandes, M. S. E. Moursi, N. Hatziargyriou, and S. E. Khatib, "A review of power system flexibility with high penetration of renewables," *IEEE Trans. Power Syst.*, vol. 34, no. 4, pp. 3140–3155, Jul. 2019, doi: 10.1109/TPWRS.2019.2897727.
[6] Y.-K. Wu, L.-T. Chang, T.-Y. Hsieh, and B.-S. Jan, "A review of flexibility requirement of electric generators in high wind power penetration systems," in *Proc. Int. Conf. Appl. Syst. Innov. (ICASI)*, Sapporo, Japan, May 2017, pp. 1890–1893, doi: 10.1109/ICASI.2017.7988317.
[7] I. G. Marneris and P. N. Biskas, "Short-term scheduling of power system flexibility to address real-time ramping requirements," in *Proc. IEEE Int. Energy Conf. (ENERGYCON)*, Leuven, Belgium, Apr. 2016, pp. 1–6, doi: 10.1109/ENERGYCON.2016.7513925.
[8] J. Endrenyi, *Reliability Modeling in Electric Power Systems*. Hoboken, NJ, USA: Wiley, 1979.
[9] R. Billinton and R. N. Allan, *Reliability Evaluation of Power Systems*, 2nd ed. New York, NY, USA: Springer, 1996.
[10] R. Billinton and M. Fotuhi-Firuzabad, "A basic framework for generating system operating health analysis," *IEEE Trans. Power Syst.*, vol. 9, no. 3, pp. 1610–1617, Aug. 1994, doi: 10.1109/59.336097.
[11] S. Y. Abujarad, M. W. Mustafa, J. J. Jamian, and A. M. Abdilahi, "Flexibility quantification for thermal power generators using deterministic metric for high renewable energy penetration," in *Proc. IEEE Int. Conf. Power Energy (PECon)*, Melaka, Malaysia, Nov. 2016, pp. 580–584, doi: 10.1109/PECON.2016.7951627.
[12] T. Heggarty, J.-Y. Bourmaud, R. Girard, and G. Kariniotakis, "Quantifying power system flexibility provision," *Appl. Energy*, vol. 279, Dec. 2020, Art. no. 115852, doi: 10.1016/j.apenergy.2020.115852.
[13] C. Anderson and J. Matevosyan, "Flexibility studies in system planning at ERCOT," in *Proc. IEEE Power Energy Soc. Gen. Meeting*, Chicago, IL, USA, Jul. 2017, pp. 1–5, doi: 10.1109/PESGM.2017.8273880.
[14] E. Lannoye, A. Tuohy, P. Daly, D. Flynn, and M. O'Malley, "Assessing power system flexibility for variable renewable integration: A flexibility metric for long-term system planning," *CIGRE Sci. Eng.*, vol. 3, p. 26, Oct. 2015.
[15] I. F. Abdin and E. Zio, "An integrated framework for operational flexibility assessment in multi-period power system planning with renewable energy production," *Appl. Energy*, vol. 222, pp. 898–914, Jul. 2018, doi: 10.1016/j.apenergy.2018.04.009.
[16] Z. Lu, H. Li, and Y. Qiao, "Probabilistic flexibility evaluation for power system planning considering its association with renewable power curtailment," *IEEE Trans. Power Syst.*, vol. 33, no. 3, pp. 3285–3295, May 2018, doi: 10.1109/TPWRS.2018.2810091.

[17] Y.-K. Wu, W.-S. Tan, S.-R. Huang, Y.-S. Chiang, C.-P. Chiu, and C.-L. Su, "Impact of generation flexibility on the operating costs of the Taiwan power system under a high penetration of renewable power," *IEEE Trans. Ind. Appl.*, vol. 56, no. 3, pp. 2348–2359, May 2020, doi: 10.1109/TIA.2020.2974435.
[18] J. Ma, V. Silva, R. Belhomme, D. S. Kirschen, and L. F. Ochoa, "Evaluating and planning flexibility in sustainable power systems," *IEEE Trans. Sustain. Energy*, vol. 4, no. 1, pp. 200–209, Jan. 2013, doi: 10.1109/TSTE.2012.2212471.
[19] H. Berahmandpour, S. M. Kuhsari, and H. Rastegar, "A new approach on development of power system operational flexibility index by combination of generation unit flexibility indices," *AUT J. Electr. Eng.*, vol. 53, no. 1, p. 3, Jun. 2021, doi: 10.22060/eej.2020.18574.5358.
[20] S. Abujarad, M. W. Mustafa, J. J. Jamian, A. M. Abdilahi, J. D. M. De Kooning, J. Desmet, and L. Vandevelde, "An adjusted weight metric to quantify flexibility available in conventional generators for low carbon power systems," *Energies*, vol. 13, no. 21, p. 5658, Oct. 2020, doi: 10.3390/en13215658.
[21] Y. Wen, C. Y. Chung, and X. Ye, "Enhancing frequency stability of asynchronous grids interconnected with HVDC links," *IEEE Trans. Power Syst.*, vol. 33, no. 2, pp. 1800–1810, Mar. 2018, doi: 10.1109/TPWRS.2017.2726444.
[22] H. Huang, M. Zhou, S. Zhang, L. Zhang, G. Li, and Y. Sun, "Exploiting the operational flexibility of wind integrated hybrid AC/DC power systems," *IEEE Trans. Power Syst.*, vol. 36, no. 1, pp. 818–826, Jan. 2021, doi: 10.1109/TPWRS.2020.3014906.
[23] F. Pourahmadi, S. H. Hosseini, and M. Fotuhi-Firuzabad, "Economically optimal uncertainty set characterization for power system operational flexibility," *IEEE Trans. Ind. Informat.*, vol. 15, no. 10, pp. 5456–5465, Oct. 2019, doi: 10.1109/TII.2019.2906058.
[24] A. A. Thatte and L. Xie, "A metric and market construct of inter-temporal flexibility in time-coupled economic dispatch," *IEEE Trans. Power Syst.*, vol. 31, no. 5, pp. 3437–3446, Sep. 2016, doi: 10.1109/TPWRS.2015.2495118.
[25] H. Nosair and F. Bouffard, "Flexibility envelopes for power system operational planning," *IEEE Trans. Sustain. Energy*, vol. 6, no. 3, pp. 800–809, Jul. 2015, doi: 10.1109/TSTE.2015.2410760.
[26] T. G. Hlalele, R. M. Naidoo, R. C. Bansal, and J. Zhang, "Multi-objective stochastic economic dispatch with maximal renewable penetration under renewable obligation," *Appl. Energy*, vol. 270, Jul. 2020, Art. no. 115120, doi: 10.1016/j.apenergy.2020.115120.
[27] J. Yang, L. Zhang, X. Han, and M. Wang, "Evaluation of operational flexibility for power system with energy storage," in *Proc. Int. Conf. Smart Grid Clean Energy Technol. (ICSGCE)*, Chengdu, China, Oct. 2016, pp. 187–191, doi: 10.1109/ICSGCE.2016.7876050.
[28] R. Udawalpola, T. Masuta, T. Yoshioka, K. Takahashi, and H. Ohtake, "Reduction of power imbalances using battery energy storage system in a bulk power system with extremely large photovoltaics interactions," *Energies*, vol. 14, no. 3, p. 522, Jan. 2021, doi: 10.3390/en14030522.
[29] M. Carrion and J. M. Arroyo, "A computationally efficient mixed-integer linear formulation for the thermal unit commitment problem," *IEEE Trans. Power Syst.*, vol. 21, no. 3, pp. 1371–1378, Aug. 2006, doi: 10.1109/TPWRS.2006.876672.
[30] D. L. H. Aik, "A general-order system frequency response model incorporating load shedding: Analytic modeling and applications," *IEEE Trans. Power Syst.*, vol. 21, no. 2, pp. 709–717, May 2006, doi: 10.1109/TPWRS.2006.873123.
[31] P. M. Anderson and M. Mirheydar, "A low-order system frequency response model," *IEEE Trans. Power Syst.*, vol. 5, no. 3, pp. 720–729, Aug. 1990, doi: 10.1109/59.65898.
[32] *TEPCO: Electricity Forecast*. Accessed: Aug. 21, 2022. [Online]. Available: https://www4.tepco.co.jp/en/forecast/html/index-e.html

AKILA HERATH (Student Member, IEEE) received the B.Sc.Eng. degree (Hons.) from the Department of Electrical and Electronic Engineering, Faculty of Engineering, University of Peradeniya, in 2017, where he is currently pursuing the M.Phil. degree in electrical and electronic engineering.

M. A. MOHAMMED MANAZ (Member, IEEE) received the B.Sc.Eng. (Hons.) and M.Phil. degrees in electrical and electronic engineering from the University of Peradeniya, Sri Lanka, in 2010 and 2014, respectively, and the Ph.D. degree in electrical engineering from the National Sun Yat-sen University, Taiwan, in 2019. He is currently an Assistant Professor with the National Sun Yat-sen University.

KITHSIRI M. LIYANAGE (Senior Member, IEEE) received the B.Sc.Eng. degree (Hons.) from the University of Peradeniya, Sri Lanka, in 1983, and the M.Eng. and Dr.Eng. degrees from The University of Tokyo, Japan, in 1988 and 1991, respectively. He has held positions at The University of Tokyo, University of Washington, Center for Advanced Power and Environmental Technology (APET), The University of Tokyo, and University of Ruhuna, Sri Lanka. He is currently a Professor with the University of Peradeniya.

TAISUKE MASUTA (Member, IEEE) received the Graduate degree from the Department of Electrical Engineering, Faculty of Engineering, The University of Tokyo, in 2005, the master's degree from the Department of Electrical Engineering, Graduate School of Engineering, in 2007, and the Ph.D. degree from the Department of Electrical Engineering and Information Systems, Graduate School of Engineering, The University of Tokyo, in 2012. He was employed at Tokyo Electric Power Company Inc. He was worked with the National Institute of Advanced Industrial Science and Technology. In 2014, he was worked with the Institute of Applied Energy. In 2016, he was worked with the Department of Electrical and Electronic Engineering, Faculty of Science and Technology, Meijo University, where he is currently a Professor.

CHAN-NAN LU (Fellow, IEEE) received the Ph.D. degree from Purdue University, in 1987. He has held positions at General Electric Company, and Harris Corporation Control Division. He is currently a Professor with the Department of Electrical Engineering, National Sun Yat-Sen University, Taiwan. His research interest includes power system operations.

KOJI NISHIO received the Graduate degree from the Department of Electrical and Electronic Engineering, Faculty of Science and Technology, Meijo University, in 2020, and the master's degree from the Department of Electrical and Electronic Engineering, Graduate School of Science and Technology, in 2022.